Title
Enhancement of Boiling with Scalable Sandblasted Surfaces

Journal
ACS Applied Materials & Interfaces, 14(7)

ISSN
1944-8244

Authors
Song, Youngsup
Wang, Chi
Preston, Daniel J
et al.

Publication Date
2022-02-23

DOI
10.1021/acsami.1c22207

Enhancement of Boiling with Scalable Sandblasted Surfaces

Youngsup Song,[1] Chi Wang,[2] Daniel J. Preston,[3] Guanyu Su,[2] Md Mahamudur Rahman,[4] Hyeongyun Cha,[1] Jee Hyun Seong,[2] Bren Philips,[2] Matteo Bucci,[2] Evelyn N. Wang[1,]*

[1]Department of Mechanical Engineering, Massachusetts Institute of Technology, Cambridge, Massachusetts 02139, USA

[2]Department of Nuclear Science and Engineering, Massachusetts Institute of Technology, Cambridge, Massachusetts 02139, USA

[3]Department of Mechanical Engineering, William Marsh Rice University, Houston, Texas 77005, USA

[4]Department of Mechanical Engineering, University of Texas at El Paso, El Paso, Texas, 79968, USA

[*]Author to whom correspondence should be addressed: enwang@mit.edu

KEYWORDS

Pool Boiling, Power Plant, Critical Heat Flux, Heat Transfer Coefficient, Surface Engineering

Abstract

Surface engineering has been leveraged by researchers to enhance boiling heat transfer performance, with benefits ranging from improved thermal management to more efficient power generation. While engineered surfaces fabricated using cleanroom processes have shown promising boiling results, scalable methods for surface engineering are still limited despite most real-world industry-scale applications involving large boiling areas. In this work, we investigate the use of sandblasting as a scalable surface engineering technique for enhancement of pool boiling heat transfer. We vary the size of an abrasive Al_2O_3 sandblasting media (25, 50, 100, and 150 μm) and quantify its effects on silicon surface conditions and boiling characteristics. The surface morphology and capillary wicking performance are characterized by optical profilometry and capillary-rise tests, respectively. Pool boiling results and surface characterization reveal that surface roughness and volumetric wicking rate increase with the abrasive size, which results in improvements in critical heat flux and heat transfer coefficient of up to 192.6% and 434.3% compared to a smooth silicon surface, respectively. The significant enhancement achieved with sandblasted surfaces indicates that sandblasting is a promising option for improving boiling performance in industry-scale applications.

1. Introduction

Boiling is a vital process in industrial applications, particularly where steam generation is required, such as power plants, water purification, food and chemical processing, and sterilization. For example, the majority of electrical power is generated in power plants that operate using steam cycles, in which various resources (e.g., natural gas, coal, nuclear energy, biomass, and geothermal energy) are used to produce steam that turns turbines attached to generators.[1] The enhancement of boiling performance by engineering boiling surfaces has therefore been studied extensively due to its practical importance across industries. Particularly, cleanroom-processed micro- and nanostructures have been exploited for systematic studies of structural effects on boiling heat transfer enhancement.[2-10] For example, surfaces with rough, permeable structures such as micropillars and nanowires have enabled significant enhancements in the operational limit of nucleate boiling, i.e., the critical heat flux (CHF).[2-4, 7-8] The CHF enhancement is of particular interest for the nuclear reactor safety. When an applied heat flux exceeds the CHF, an instantaneous formation of vapor films over the surface drastically increase the thermal resistance, which leads to thermal runaway and a crucial failure of a boiling system. Nucleation-engineered surfaces such as microcavity arrays, on the other hand, have shown improved heat transfer efficiency as quantified by the heat transfer coefficient (HTC).[5-6] Despite the significant enhancement of pool boiling heat transfer, these cleanroom-processed surfaces are not suitable for industry-scale applications due to the limited scalability. Solution-based surface modifications such as surface oxidation, wet etching, synthesis of nanowires, and coatings of nanoporous layers may provide better scalability than clean-room processes;[11-16] however, these approaches are often limited to a specific material due to the need for chemical compatibility, and nanomaterials have limited durability that may preclude use in industrial applications.[17]

In this work, we show a sandblasting process as a scalable surface structuring technique for the enhancement of pool boiling heat transfer for industry-scale boiling applications. Sandblasting is a purely physical bombardment process free of chemical compatibility constraints; therefore, it is applicable to a wide range of materials including Zircaloy, which is commonly used in nuclear reactors.[18-20] This simple process also allows sandblasting to be scaled up and widely used in industry for surface roughening or smoothening.[21] In fact, sandblasting has already been utilized as a physical texturing method to study the effects of surface roughness on boiling heat transfer in previous studies.[22-29] The detailed analysis on the structural characteristics of sandblasted surfaces and their effects on boiling heat transfer, however, are still lacking. In this work, we investigated the mechanism of boiling enhancement of sandblasted surfaces by characterizing their surface area ratios and capillary-driven wickabilities, which were found to be critical for CHF during pool boiling.[30] The pool boiling experiments were conducted with water on silicon surfaces sandblasted by aluminum oxide particles. We chose silicon as a test surface because of its compatibility with our boiling setup as well as abundant pool boiling literature data on silicon that we can compare with our results. The abrasive media size was varied (25, 50, 100, and 150 µm). Surface morphology and capillary-wicking performance were characterized by an optical profilometer and capillary-rise tests. Surfaces sandblasted by larger abrasives (up to 150 µm) exhibited higher roughness and volumetric wicking rate, resulting in greater enhancements of CHF and HTC values.

2. Preparation and characterization of sandblasted surfaces

2.1. Sandblasting process

Sandblasted boiling samples were prepared based on a 650-µm-thick silicon substrate with thermally grown 1 µm SiO_2 layers on both sides. The top SiO_2 layer was completely etched by reactive-ion etching to expose underlying silicon before sandblasting with a laboratory-scale sandblaster (AccuFlo AF10 Standard Tank, Comco Inc.). A schematic of the sandblasting process is shown in Figure 1a. The blasting nozzle was mounted on an XY linear stage and is raster scanned over the surfaces with a constant line-pitch (p_l) of 1.1 mm and a sweeping speed (v) of 6.1 cm/s, where its motion is controlled with a microcontroller (Arduino Uno). The nozzle-to-sample distance (d_n) and blasting pressure (P) were fixed at 12.7 mm and 827 kPa (120 psi), respectively. In order to create different structural features, Al_2O_3 abrasives with four different nominal sizes (25, 50, 100, and 150 μm) were tested. Figure 1b shows a pile of Al_2O_3 abrasives, where each abrasive has a blocky and sharp shape as shown in scanning electron microscope (SEM) images (Figure 1c – 1f). The nominal size of abrasives was calculated as an equivalent diameter sphere by laser diffraction patterns (HELOS, Sympatec).

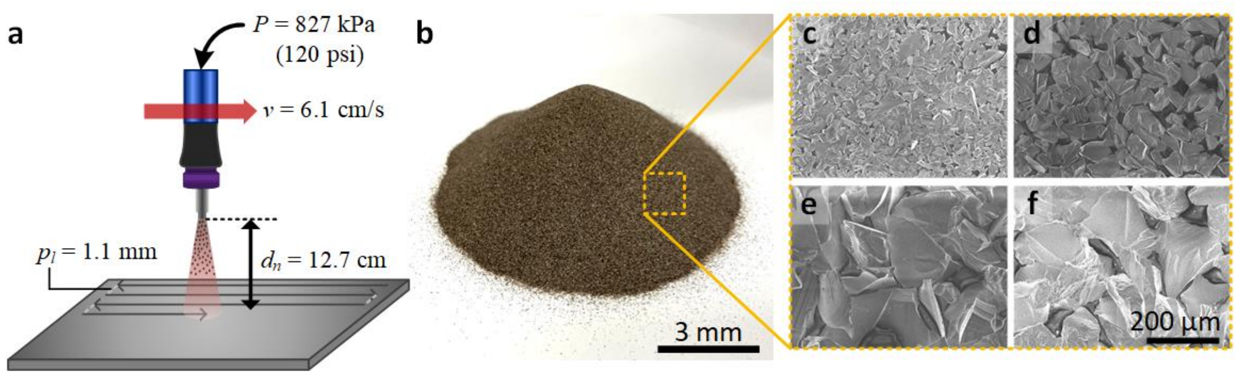

Figure 1. Sandblasting process and abrasives. (a) A schematic of the sandblasting process. Sandblasting pressure (P), sweeping speed (v), line-pitch (p_l), and nozzle-to-sample distance (d_n) were fixed while changing the Al_2O_3 abrasive size from 25 to 150 μm. (b) Optical image of a pile of sandblasting abrasives. (c – f) Scanning electron microscope images of sandblasting abrasives of 25, 50, 100, and 150 μm, respectively.

2.2. Morphology of sandblasted surfaces

The surface structures created by the sandblasting process were analyzed quantitatively by an optical profilometer (Non-contact 3D profiler CCI, Taylor Hobson) as shown in Figure 2. Figure 2a–d show the three-dimensional profile images of surfaces sandblasted by 25, 50, 100, and 150 μm, respectively. The roughness (r), defined as the ratio of actual surface area to projected area, has been proposed as a critical surface feature determining CHF values in previous works.[2, 31] Figure 2e shows the change in r along with the arithmetic-mean roughness (R_a) and root-mean-square roughness (R_q) as functions of blasting abrasive size. We measured the roughness parameters at ten different randomly selected positions on each surface. The average and standard deviation values were used as data points and error bars, respectively. All three parameters increased noticeably as abrasive size increased from 25 to 100 μm, while the differences of parameters between the cases of 100 and 150 μm abrasives were insignificant and within error bar ranges. The plots of surface profiles in a horizontal direction are shown in Figure 2f–h. Grey regions represent the overlapped profiles over the other horizontal direction, from which the peak-to-valley amplitude Δz was characterized. The peak-to-valley amplitude increased with the abrasive size. A blue line in each plot shows a typical profile at a specific position in the other horizontal direction. SEM and energy-dispersive X-ray (EDS) images of sandblasted surfaces are provided in Section I of the Supporting Information.

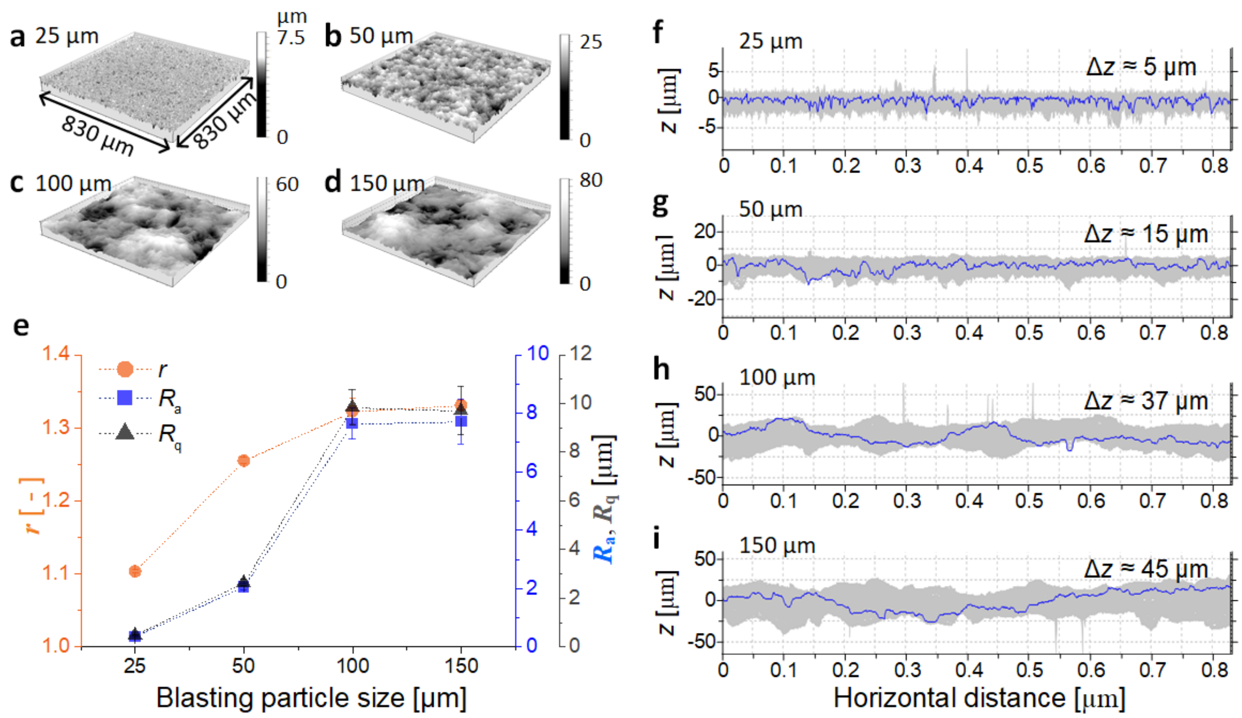

Figure 2. Surface structures characterized by an optical profilometer. (a–d) Three-dimensional profiles of surfaces sandblasted by 25, 50, 100, and 150 µm, respectively. (e) Surface area ratio (*r*, orange circles), arithmetic-mean roughness (R_a, blue squares), and root-mean-square roughness (R_q, gray triangles) as functions of blasting abrasive size. Error bars represent the standard deviations of ten different measurements at random positions on each surface. (f–i) Profile plots in one of the horizontal directions of surfaces sandblasted by 25, 50, 100, and 150 µm, respectively. The blue line and grey region indicate a profile at a fixed position and the overlaps of all profiles in the perpendicular horizontal direction, respectively. The peak-to-valley amplitude Δz was characterized based on the grey region.

2.3. Wickability of sandblasted surfaces

In addition to surface roughness r, the surface wickability has been found to be a good indicator for pool boiling CHF enhancements.[3-4, 32] To characterize the wickability of sandblasted surfaces, we performed capillary rise tests (Figure 3a). A sample was moved vertically toward the reservoir of water until it came in contact, resulting in upward capillary rise flow through the sandblasted surface. The propagation speed of the capillary rise was captured with a digital camera at 30 frames per second. Figure 3c shows the time-lapse images of propagating wicking front on the surface sandblasted by 150 μm abrasives as an example. Once the sample contacted the surface of water, a capillary meniscus formed (highlighted in white dashed lines) first, and liquid propagated (wicking front shown with yellow dashed lines) upward with the speed (u) associated with the balance between capillary pressure and viscous resistance. This liquid propagation through porous sandblasted structures can be described by Darcy's law (or the Brinkman equation, if viscous shearing is the dominant flow resistance compared to structural permeability) as

$$\frac{dx}{dt} = \frac{K_{\mathrm{B}}}{\mu}\frac{\Delta P_{\mathrm{cap}}}{x}. \quad (1)$$

Here x, t, and μ are the propagation distance, time, and dynamic viscosity of liquid. P_{cap} and K_{B} are the capillary pressure and effective permeability that structured surfaces exhibit. By solving the equation with initial condition $x(t=0)=0$, the propagation distance (x) can be expressed as a square root function of time (t) with a propagation coefficient G as a proportional coefficient, i.e.,

$$x = \sqrt{\frac{2P_{\mathrm{cap}}K_{\mathrm{B}}}{\mu}t} = \mathrm{G}\sqrt{t}. \quad (2)$$[33]

The measured propagation distances are shown in Figure 3b as a function of time along with fittings of square root function. Propagation coefficient G values derived from curve fitting (shown next to each curve) increased with the abrasive size, indicating a silicon surface sandblasted by larger abrasives (up to 150 μm) exhibited better surface wickability.

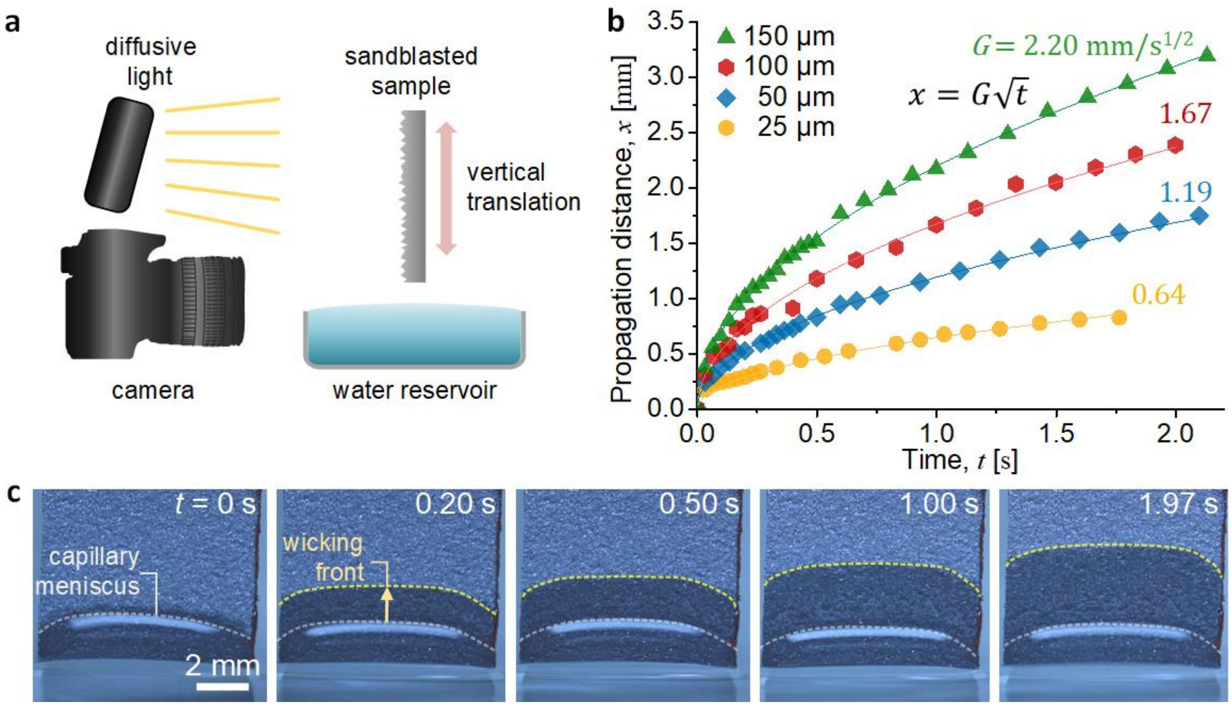

Figure 3. Surface wickability measurements of sandblasted surfaces. (a) Schematic of experimental setup for wickability measurement. A sandblasted surface is immersed vertically into the reservoir of water while a digital camera captures the speed of capillary rise at 30 frames per second. (b) The propagation distance (x) of capillary rise plotted as a function of time (t). The data points and lines represent experimental measurements and the fitting of square root functions, respectively. Propagation coefficient values (G) for each surface are shown next to the

corresponding case. (c) Time-lapse images show an example of the wicking front of water on the surface sandblasted by 150 µm Al_2O_3 abrasives.

3. Pool boiling experiments

The pool boiling heat transfer characteristics of the sandblasted surfaces were characterized with high-purity deionized water at saturated atmospheric conditions. On the back side of each boiling sample, a 100-nm-thick serpentine Pt heater was patterned by a lift-off process to define the 10 × 10 mm^2 heating area, which also served as a resistive temperature detector for temperature characterization. All test samples were cleaned by solvents (acetone, methanol, and isopropyl alcohol) and argon plasma before boiling to remove organic contaminants.[34] The details of the experimental setup and boiling heat transfer characterization methods are provided in Section II of the Supporting Information.

Figure 4a shows pool boiling curves, i.e., heat flux (q'') as a function of wall superheat (ΔT_w), of a smooth silicon surface and the sandblasted silicon surfaces. During the experiments, we gradually increased the input heat flux by controlling the applied voltage up to the CHF point, at which point thermal runaway occurred as indicated with an arrow in the plot. HTC, i.e., the slope of a point from the origin on a boiling curve (by definition), is also plotted as a function of heat flux in Figure 4b. All sandblasted surfaces demonstrated the increase of CHF and HTC as the abrasive size increased. This result is similar to a previous work that has shown the monotonic increase of CHF and HTC with the increase of arithmetic-mean roughness of copper surfaces roughened by sandpapers.[35] CHF values monotonically increased from 65.1 W/cm^2 for the smooth surface to 103.8, 135.0, 160.1, and 190.5 W/cm^2 for 25, 50, 100, and 150 µm abrasives, respectively, resulting in up to 192.6% CHF enhancement. It is interesting to note that the surface sandblasted by 50 µm abrasives showed higher HTC values than the surface sandblasted by 100 µm abrasives at the early stage ($\Delta T_W < {\sim}25°C$), which may be associated with the optimal cavity size for the earlier onset of nucleate boiling.[36] A future parametric study including other sandblasting parameters may provide a detailed analysis about the early stage behavior of nucleate boiling. Nonetheless, the HTC values at CHF points showed a similar trend with CHF, i.e., an increase in HTC with increasing abrasive size. The maximum HTC value at CHF was 14.3 kW/m^2 for the smooth silicon, which increased to 29.3, 41.6, 52.6, and 76.3 kW/m^2 for surfaces sandblasted by 25, 50, 100, and 150 µm abrasives, respectively, resulting in up to 433.6% enhancement. The CHF and HTC enhancements achieved with sandblasted silicon surfaces were comparable to that of cleanroom-processed surfaces,[2, 4-6] indicating promise for the use of a sandblasting process as a scalable surface engineering technique for boiling heat transfer enhancement.

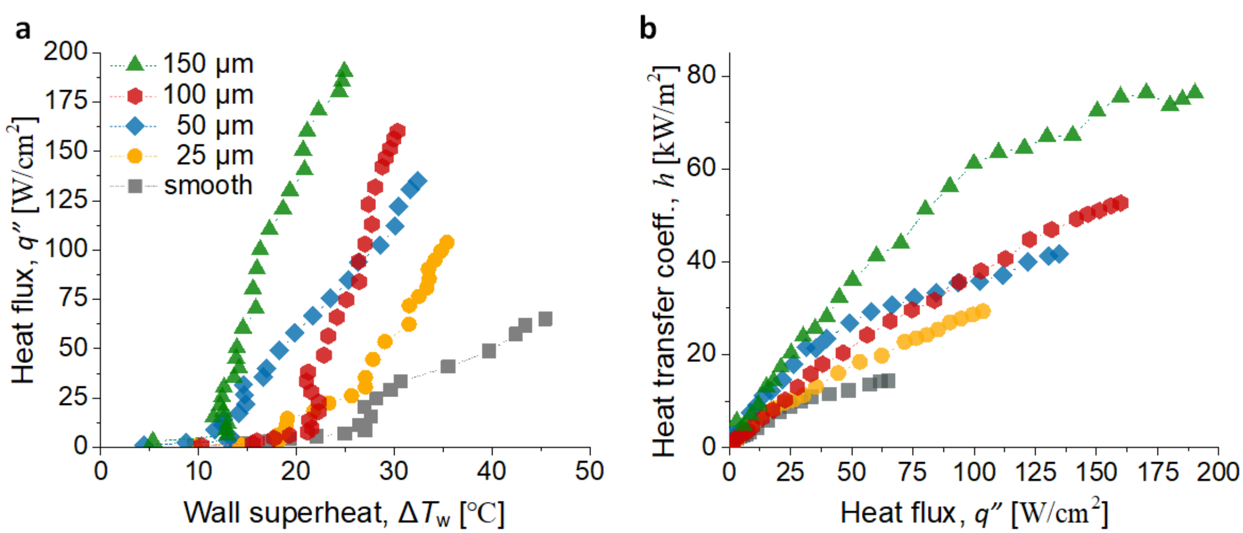

Figure 4. Pool boiling results of a smooth and sandblasted silicon surfaces. (a) Pool boiling curves of water. (b) Heat transfer coefficient as a function of heat flux. The experimental uncertainty was smaller than the marker size.

3.3. Mechanism of heat transfer coefficient enhancement

We attribute the HTC enhancement to the potential increase in the nucleation site density and bubble departure frequency on sandblasted surfaces. As shown in surface profile images (Figure 2a – 2d), the sandblasting process created rough cavities, which could serve as nucleation sites. In addition, capillary-driven wicking may accelerate bubble departure frequency by providing the additional evaporation from thin wicked liquid. Considering high-pressure boiling applications such as nuclear reactors, it is important to compare the relative contribution of nucleation site density and bubble departure frequency to the HTC enhancement of sandblasted surfaces. As pressure increases, the nucleation energy barrier decreases and thus, the structural effects on nucleation site density can be diminished.[37] On this account, if the dominant mechanism for the HTC enhancement is the increase of nucleation site density, sandblasted surfaces may not enhance HTC effectively for high-pressure boiling applications. To determine the dominant mechanism, between nucleation and frequency, we plotted the maximum HTC values against roughness (r) and wicking speed ($P_{\mathrm{cap}}K_{\mathrm{B}}$) in Figure 5. The surface roughness can be directly obtained from the optical profile measurement (Figure 2) and the wicking speed $P_{\mathrm{cap}}K_{\mathrm{B}}$ can be obtained from the capillary-rise test (Figure 3) according to Darcy's law as $P_{\mathrm{cap}}K_{\mathrm{B}} = \mu G^2/2$, where μ is the dynamic viscosity of water. The maximum HTC values generally increase with both roughness and wicking speed. Samples blasted by 100 µm and 150 μm abrasives, however, show a stronger correlation of HTC values with wicking speed than roughness, indicating that the increased bubble departure frequency induced by wicking may play a more important role for the HTC enhancement.

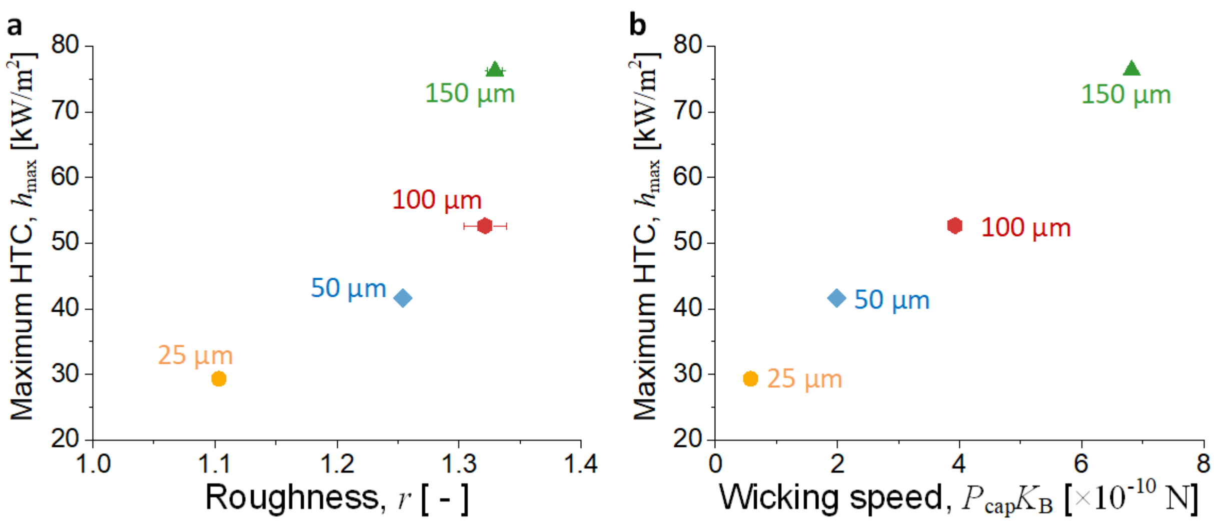

Figure 5. Relationships of maximum heat transfer coefficient with (a) roughness (r) and (b) wicking speed ($P_{cap}K_B = \mu G^2 \Delta z/2$) of sandblasted surfaces. Sandblasting abrasive size is indicated next to each data point.

3.4. Critical heat flux and surface characteristics

While past work has shown that roughness and wickability can enhance CHF enhancement, a recent study based on cleanroom-processed micropillar arrays showed that a single parameter such as roughness (r) or wicking speed ($P_{cap}K_B$) is not sufficient to describe the CHF enhancement of hemi-wicking surfaces. Instead, the unified descriptor ($\xi^n P_{cap}K_B h$) showed an improved linear correlation with the CHF, where ξ, h, and n are thin film density, thickness of wick layer, and experimental fitting parameter, respectively.[30] This unified descriptor represents the combined effects of enhanced evaporation from the liquid thin films around structures and the delay of dry-out by capillary wicking. Here we rearrange the unified descriptor as $(\xi^{\mathrm{n}}h)(P_{\mathrm{cap}}K_{\mathrm{B}})$, where $\xi^{\mathrm{n}}h$ can be approximated as surface roughness r. Accordingly, we approximate the unified descriptor as $rP_{\mathrm{cap}}K_{\mathrm{B}}$. In Figure 6, we compared the correlations of CHF with roughness (Figure 6a), wicking speed (Figure 6b), and the unified descriptor (Figure 6c). CHF values of sandblasted surfaces exhibited monotonic increases with all three parameters. The unified descriptor, however, showed the best correlation with the CHF among the three parameters (Figure 6c), which is consistent with the previous study with micropillars.[30] Note that sandblasted surfaces have artificial nucleation sites such as cavities as opposed to micropillar arrays, which can exhibit more complex CHF enhancement mechanisms associated with the increased nucleation site density.[6] Nonetheless, the consistent linear correlation of CHF values of sandblasted surfaces with the unified descriptor suggests that sandblasted surfaces can be optimized for the CHF by controlling the unified descriptor in future work.

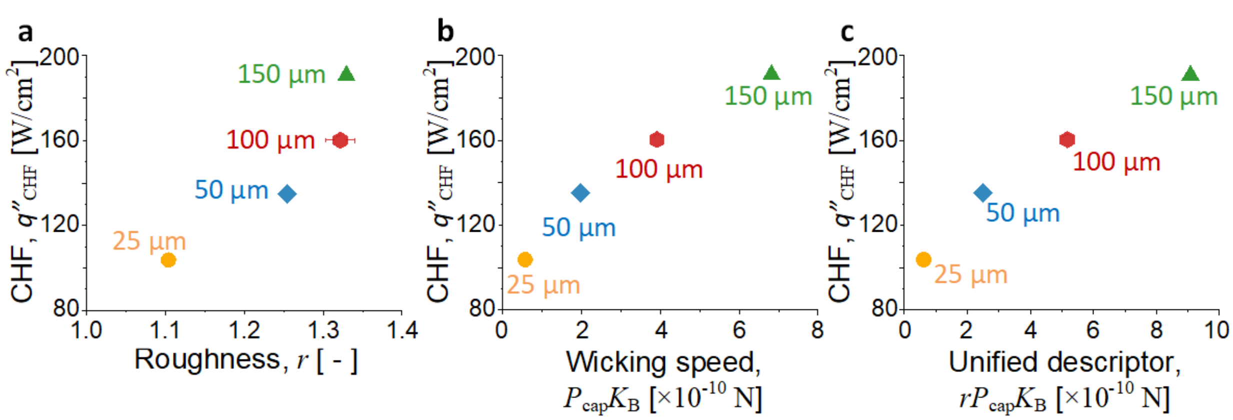

Figure 6. Relationships of critical heat flux with (a) roughness (r), (b) wicking speed ($P_{\mathrm{cap}}K_{\mathrm{B}} = \mu G^2 \Delta z/2$), and (c) the unified descriptor ($rP_{\mathrm{cap}}K_{\mathrm{B}}$) of sandblasted surfaces. Sandblasting abrasive size is indicated next to each data point.

4. Conclusions

In this work, we showed that a sandblasting process is promising as a surface engineering technique for enhancement of pool boiling heat transfer in industry-scale applications. We fabricated sandblasted silicon surfaces using Al_2O_3 abrasives with four different sizes, i.e., 25, 50, 100, and 150 µm. The morphology of the sandblasted surfaces was quantitatively characterized using an optical profilometer; all three measures of roughness (r, R_a, and R_q) increased noticeably as abrasive size increased from 25 to 100 µm, while the difference of roughness parameters between the 100 and 150 µm cases is marginal. Surface wickability was characterized as a propagation coefficient of one-dimensional capillary flow, and showed increasing trend of surface wickability with increasing abrasive size. Pool boiling performance of sandblasted surfaces was subsequently characterized with high-purity deionized water at saturated atmospheric conditions. Sandblasted surfaces demonstrated significant CHF and HTC enhancements compared to a smooth surface. The highest enhancement was achieved with the surface sandblasted by 150 µm abrasives, where CHF and HTC were enhanced up to 192.6% and 433.6%, respectively. The CHF enhancement of sandblasted surfaces showed a stronger correlation with the unified descriptor, compared to that with roughness and wicking speed alone.[32] In this work, we used silicon as a base material, of which the heat transfer enhancement is limited to specific applications, such as electronics cooling. To further demonstrate the applicability of sandblasting for heat transfer enhancements of nuclear power plants, investigations of durability and boiling performance under high pressure with commercial materials for nuclear reactors such as Zircaloy is needed, which will be pursued in future work. Furthermore, we expect that further enhancements can be achieved by investigating an optimal sandblasting condition. For example, we tested the abrasive size up to 150 µm in this study, but there can be an optimal abrasive size larger than 150 µm. In addition, an optimal boiling surface with higher roughness and volumetric wicking rate can be found through a parametric study including the other sandblasting parameters such as pressure (P), sweeping speed (v), line-pitch (p_l), and nozzle-to-sample distance (d_n). Nevertheless, the significant enhancement of boiling heat transfer demonstrated in this work promises the potential of a sandblasting process for industry-scale boiling applications.

Authors' Contributions

Y. Song and E. N. Wang conceived the idea. Y. Song, C. Wang, G. Su, and M. M. Rahman conducted boiling experiments. Y. Song and D. J. Preston performed EDS analysis. Y. Song and H. Cha fabricated sandblasted surfaces. Y. Song and J. H. Seong characterized surface morphology with optical profilometry. Y. Song characterized surface wickability. B. Philips, M. Bucci, and E. N. Wang guided the work. D. J. Preston, M. Bucci, and E. N. Wang acquired the financial supports. The manuscript was written through contributions of all authors.

Supporting Information

Scanning electron microscope and energy-dispersive x-ray spectroscopy images of sandblasted surfaces; Pool boiling experimental setup and characterization

Acknowledgements

Y. Song, C. Wang, G. Su, and M. M. Rahman, B. Philips, M. Bucci, and E. N. Wang gratefully acknowledges funding received from Exelon Corporation through its membership in the MIT Energy Initiative's Low Carbon Energy Centers. Y. Song, H. Cha, and E. N. Wang acknowledge that the information, data, or work presented herein was funded in part by the Advanced Research Projects Agency-Energy (ARPA-E), U. S. Department of Energy, under Award Number DE-AR0000ABC. J. H. Seong, B. Philips, and M. Bucci acknowledge the funding support of the US Nuclear Regulatory Commission (NRC) and the Department of Energy through the Consortium for the Advanced Simulation of Light Water Reactors (CASL). D. J. Preston acknowledges funding support from the Rice University Faculty Initiatives Fund.

References

1. *Annual Energy Outlook 2020*; Washington, DC, **2020**; pp 1-162.
2. Chu, K.-H.; Enright, R.; Wang, E. N. Structured Surfaces for Enhanced Pool Boiling Heat Transfer. *Appl. Phys. Lett.* **2012**, *100*, 241603.
3. Rahman, M. M.; Ölçeroğlu, E.; McCarthy, M. Role of Wickability on the Critical Heat Flux of Structured Superhydrophilic Surfaces. *Langmuir* **2014**, *30*, 11225-11234.
4. Dhillon, N. S.; Buongiorno, J.; Varanasi, K. K. Critical Heat Flux Maxima During Boiling Crisis on Textured Surfaces. *Nat. Commun.* **2015**, *6*, 8247.
5. Kim, D. E.; Park, S. C.; Yu, D. I.; Kim, M. H.; Ahn, H. S. Enhanced Critical Heat Flux by Capillary Driven Liquid Flow on the Well-Designed Surface. *Appl. Phys. Lett.* **2015**, *107*, 023903.
6. Song, Y.; Gong, S.; Vaartstra, G.; Wang, E. N. Microtube Surfaces for the Simultaneous Enhancement of Efficiency and Critical Heat Flux During Pool Boiling. *ACS Appl. Mater. Interfaces* **2021**, *13*, 12629-12635.
7. Shim, D. I.; Choi, G.; Lee, N.; Kim, T.; Kim, B. S.; Cho, H. H. Enhancement of Pool Boiling Heat Transfer Using Aligned Silicon Nanowire Arrays. *ACS Appl. Mater. Interfaces* **2017**, *9*, 17595-17602.

8. Zhao, H.; Dash, S.; Dhillon, N. S.; Kim, S.; Lettiere, B.; Varanasi, K. K.; Hart, A. J. Microstructured Ceramic-Coated Carbon Nanotube Surfaces for High Heat Flux Pool Boiling. *ACS Applied Nano Materials* **2019**, *2*, 5538-5545.
9. Kong, D.; Kang, M.; Kim, K. Y.; Jang, J.; Cho, J.; In, J. B.; Lee, H. Hierarchically Structured Laser-Induced Graphene for Enhanced Boiling on Flexible Substrates. *ACS Appl. Mater. Interfaces* **2020**, *12*, 37784-37792.
10. Su, C.-Y.; Yang, C.-Y.; Jhang, B.-W.; Hsieh, Y.-L.; Sin, Y.-Y.; Huang, C.-C. Pool Boiling Heat Transfer Enhanced by Fluorinated Graphene as Atomic Layered Modifiers. *ACS Appl. Mater. Interfaces* **2020**, *12*, 10233-10239.
11. Godinez, J. C.; Fadda, D.; Lee, J.; You, S. M. Development of a Stable Boehmite Layer on Aluminum Surfaces for Improved Pool Boiling Heat Transfer in Water. *Appl. Therm. Eng.* **2019**, *156*, 541-549.
12. Nam, Y.; Sharratt, S.; Byon, C.; Kim, S. J.; Ju, Y. S. Fabrication and Characterization of the Capillary Performance of Superhydrophilic Cu Micropost Arrays. *Journal of Microelectromechanical Systems* **2010**, *19*, 581-588.
13. Honda , H.; Takamastu, H.; Wei, J. J. Enhanced Boiling of Fc-72 on Silicon Chips with Micro-Pin-Fins and Submicron-Scale Roughness. *J. Heat Transfer* **2001**, *124*, 383-390.
14. Tetreault-Friend, M.; Azizian, R.; Bucci, M.; McKrell, T.; Buongiorno, J.; Rubner, M.; Cohen, R. Critical Heat Flux Maxima Resulting from the Controlled Morphology of Nanoporous Hydrophilic Surface Layers. *Appl. Phys. Lett.* **2016**, *108*, 243102.
15. Chen, R.; Lu, M.-C.; Srinivasan, V.; Wang, Z.; Cho, H. H.; Majumdar, A. Nanowires for Enhanced Boiling Heat Transfer. *Nano Lett.* **2009**, *9*, 548-553.
16. Upot, N. V.; Mahvi, A.; Fazle Rabbi, K.; Li, J.; Jacobi, A. M.; Miljkovic, N. Scalable and Resilient Etched Metallic Micro- and Nanostructured Surfaces for Enhanced Flow Boiling. *ACS Applied Nano Materials* **2021**, *4*, 6648-6658.
17. Wilke, K. L.; Antao, D. S.; Cruz, S.; Iwata, R.; Zhao, Y.; Leroy, A.; Preston, D. J.; Wang, E. N. Polymer Infused Porous Surfaces for Robust, Thermally Conductive, Self-Healing Coatings for Dropwise Condensation. *ACS Nano* **2020**, *14*, 14878-14886.
18. Duan, Z.; Yang, H.; Kano, S.; Murakami, K.; Satoh, Y.; Takeda, Y.; Abe, H. Oxidation and Electrochemical Behaviors of Al2o3 and Zro2 Coatings on Zircaloy-2 Cladding by Thermal Spraying. *Surf. Coat. Technol.* **2018**, *334*, 319-327.
19. Olander, D. *Liquid Metal Bond for Improved Heat Transfer in Lwr Fuel Rods*; DOE/ID/14119; University of California, Berkeley: United States, **2005**.
20. Yeom, H.; Jo, H.; Johnson, G.; Sridharan, K.; Corradini, M. Transient Pool Boiling Heat Transfer of Oxidized and Roughened Zircaloy-4 Surfaces During Water Quenching. *Int. J. Heat Mass Transfer* **2018**, *120*, 435-446.
21. Thomas, E. G. How to Create an Abrasive Air Blast Room: By Following Design Criteria, You Can Meet Demands for a Clean Work Environment While Earning a Good Rol. *Metal Finishing* **2005**, *103*, 44-46.
22. Frieser, R. G.; Reeber, M. D. Surface Treatments of Silicon to Enhance Thermal Nucleation. *J. Appl. Electrochem.* **1980**, *10*, 449-457.
23. Truong, B.; Hu, L.-w.; Buongiorno, J.; McKrell, T. Modification of Sandblasted Plate Heaters Using Nanofluids to Enhance Pool Boiling Critical Heat Flux. *Int. J. Heat Mass Transfer* **2010**, *53*, 85-94.
24. Hübner, P.; Künstler, W. Pool Boiling Heat Transfer at Finned Tubes: Influence of Surface Roughness and Shape of the Fins. *International Journal of Refrigeration* **1997**, *20*, 575-582.
25. Gorenflo, D.; Danger, E.; Luke, A.; Kotthoff, S.; Chandra, U.; Ranganayakulu, C. Bubble Formation with Pool Boiling on Tubes with or without Basic Surface Modifications for Enhancement. *Int. J. Heat Fluid Flow* **2004**, *25*, 288-297.
26. Luke, A. Active and Potential Bubble Nucleation Sites on Different Structured Heated Surfaces. *Chem. Eng. Res. Des.* **2004**, *82*, 462-470.

27. Luke, A. Pool Boiling Heat Transfer from Horizontal Tubes with Different Surface Roughness. *International Journal of Refrigeration* **1997**, *20*, 561-574.
28. Ribatski, G.; Jabardo, J. M. S. Experimental Study of Nucleate Boiling of Halocarbon Refrigerants on Cylindrical Surfaces. *Int. J. Heat Mass Transfer* **2003**, *46*, 4439-4451.
29. Addy, J.; Olbricht, M.; Müller, B.; Luke, A. Pool Boiling Heat Transfer on Structured Surfaces. *Journal of Physics: Conference Series* **2016**, *745*, 032077.
30. Song, Y.; Zhang, L.; Díaz-Marín, C. D.; Cruz, S. S.; Wang, E. N. Unified Descriptor for Enhanced Critical Heat Flux During Pool Boiling of Hemi-Wicking Surfaces. *Int. J. Heat Mass Transfer* **2022**, *183*, 122189.
31. Chu, K.-H.; Soo Joung, Y.; Enright, R.; Buie, C. R.; Wang, E. N. Hierarchically Structured Surfaces for Boiling Critical Heat Flux Enhancement. *Appl. Phys. Lett.* **2013**, *102*, 151602.
32. Ahn, H. S.; Park, G.; Kim, J. M.; Kim, J.; Kim, M. H. The Effect of Water Absorption on Critical Heat Flux Enhancement During Pool Boiling. *Exp. Therm Fluid Sci.* **2012**, *42*, 187-195.
33. Xiao, R.; Enright, R.; Wang, E. N. Prediction and Optimization of Liquid Propagation in Micropillar Arrays. *Langmuir* **2010**, *26*, 15070-15075.
34. Song, Y.; Zhang, L.; Liu, Z.; Preston, D. J.; Wang, E. N. Effects of Airborne Hydrocarbon Adsorption on Pool Boiling Heat Transfer. *Appl. Phys. Lett.* **2020**, *116*, 253702.
35. Kim, J.; Jun, S.; Laksnarain, R.; You, S. M. Effect of Surface Roughness on Pool Boiling Heat Transfer at a Heated Surface Having Moderate Wettability. *Int. J. Heat Mass Transfer* **2016**, *101*, 992-1002.
36. Hsu, Y. Y. On the Size Range of Active Nucleation Cavities on a Heating Surface. *J. Heat Transfer* **1962**, *84*, 207-213.
37. Dahariya, S.; Betz, A. R. High Pressure Pool Boiling: Mechanisms for Heat Transfer Enhancement and Comparison to Existing Models. *Int. J. Heat Mass Transfer* **2019**, *141*, 696-706.

Table of Contents (ToC)